Determination of the Axial Electron Mobility Profile in the PPS®X000-LM Thruster

L Garrigues, J Pérez-Luna, Juslan LO, G J M Hagelaar, J P Boeuf, S Mazouffre

Determination of the Axial Electron Mobility Profile in the PPS®X000-LM Thruster

IEPC-2009-082

Presented at the 31st International Electric Propulsion Conference,
University of Michigan • Ann Arbor, Michigan • USA
September 20 – 24, 2009

L. Garrigues[*], J. Pérez-Luna[†], J.Lo[‡], G.J.M. Hagelaar[§], J.P.Boeuf[**],
Laboratoire Plasma et Conversion d'Energie, Université de Toulouse, Bâtiment 3R2, 118 route de Narbonne, 31062 Toulouse, France

and S. Mazouffre[††]
Institut de Combustion, Aérothermique, Réactivité et Environnement, 1C Avenue de la Recherche Scientifique, 45071 Orléans, France

Electron transport across the magnetic field in Hall effect thrusters is still an open question. Models have so far assumed *1/B²* or *1/B* scaling laws for the "anomalous" electron mobility, adjusted to reproduce the integrated performance parameters of the thruster. We show that models based on such mobility laws predict very different ion velocity distribution functions (IVDF) than measured by induced fluorescence (LIF). A fixed spatial mobility profile, obtained by analysis of improved LIF measurements, leads to much better model predictions of thruster performance and IVDF than *1/B²* or *1/B* mobility laws, for discharge voltages in the 500-700 V range for a 5 kW Hall thruster.

Nomenclature

A	=	channel cross section area
B	=	magnetic field magnitude
e	=	elementary electron charge
$E_\perp$	=	component of the electric field perpendicular to the magnetic field
I_d	=	discharge current
$j_{e,\perp}$	=	cross magnetic field electron current density
K	=	Bohm fitting parameter
k_m	=	electron-atom momentum transfer rate
m_a	=	xenon anode mass flow rate
m_e, m_{Xe^+}	=	electron, ion mass
N, n, n_e, n_i	=	neutral, plasma, electron and ion density
r	=	radial direction
S	=	ionization source term

[*] Research Scientist at CNRS, LAPLACE, Toulouse, France, laurent.garrigues@laplace.univ-tlse.fr.
[†] Graduate Researcher, LAPLACE, Toulouse, France, jaime.perezluna@laplace.univ-tlse.fr.
[‡] Doctoral candidate, LAPLACE, Toulouse, France, juslan.lo@laplace.univ-tlse.fr.
[§] Research Scientist at CNRS, LAPLACE, Toulouse, France, gerjan.hagelaar@laplace.univ-tlse.fr.
[**] Senior Research Scientist at CNRS, LAPLACE, Toulouse, France, jpb@laplace.univ-tlse.fr.
[††] Research Scientist at CNRS, ICARE, Orléans, France, stephane.mazouffre@cnrs-orleans.fr.

T_e = electron temperature
V_a, V_c, V = anode, cathode and electric potential
V_d = discharge voltage
$V_{i,\perp}$ = ion mean velocity perpendicular to the magnetic field
v_{max} = theoretical maximum axial ion velocity
W = electron-wall effective energy loss coefficient
x = axial direction
Xe^+ = singly charged ion
α = adjustable coefficient for electron-wall collision frequency
β = Boltzmann factor
ε = electron mean energy
Γ_i , Γ_e = ion and electron vector flux
κ = inelastic effective energy loss coefficient
$\overline{\overline{\mu}}$ = electron mobility tensor
$\mu_{e,//}$, $\mu_{e,\perp}$ = electron mobility parallel and perpendicular to the magnetic field
$\nu_{e\text{-}i}$, $\nu_{e\text{-}n}$ = electron-ion, electron-neutral collision frequency
$\nu_{e\text{-}w}$ = electron-wall collision frequency
ν_m = total electron momentum transfer collision frequency
τ = mean time between collisions
ω = cyclotron angular frequency
Ω = Hall parameter
∇ = gradient
$\nabla_\perp$ = cross magnetic field gradient

I. Introduction

In a Hall Effect Thruster (HET), the thrust is provided by the acceleration of xenon ions that originates in the efficient ionization of a xenon neutral flow in a E×B field discharge. In HETs, the ion beam velocity can reach few 10's of km.s^{-1} in comparisons with the velocity of the exhaust beam obtained in chemical thrusters limited to few km.s^{-1}. The HETs offer considerable advantages for geostationary satellites for station-keeping and orbit control[1] and for exploration probes[2] because the very high exhaust beam velocity leads to less propellant consuming. A new generation of 5kW-class Hall thrusters is now developed in order to achieve orbital manoeuvres for the next generation of large geosynchronous satellites.[3] Nevertheless, the physic involving in such kind of thruster is far from being completely mastered. Especially, there is not yet a clear theory of the so-called "anomalous electron mobility".

Indeed, in a HET configuration, electrons travel from the cathode to the anode through a E×B field region. The cross field electron mobility $\mu_{e,\perp}$ is proportional to the momentum-transfer frequency of electron-particle collisions. Due to the intense ionization in the thruster channel, the neutral density is strongly depleted in the exhaust region. The momentum transfer frequency only due to collisions between electrons and neutrals is consequently low, and can not explain the measured electron current. Different theories have been proposed to explain this anomalous electron diffusion. It has often been attributed to electron-wall interactions or plasma turbulence, or a combination between the two theories.[4-10] Fully kinetic Particle-In-Cell (PIC) simulations in the axial and azimuthal directions have demonstrated the existence of a turbulent azimuthal electric field that leads to a cross-magnetic field transport of the electrons[11, 12]. Recently, a collective light scattering diagnostic has evidenced azimuthal fluctuations of the electron density in the same wavelength range as in PIC simulations.[13] However, a scaling law of the anomalous transport has not yet been proposed. Consequently, most of hybrid models have adopted elementary formulas with tuned parameters to account for the anomalous electron transport.[4-6, 14-15]

Over the past 10-years, the time-averaged LIF technique has been extensively used and many measurements of the IVDF have been performed along the thruster channel centerline both inside and outside the thruster over a broad range of electrical power.[16-21] Recent improvements of the signal-to-noise ratio have been achieved.[22] In parallel, a technique based on the calculations of the moments of the Boltzmann equation has been recently proposed to extract the on-axis distribution of the electric field from well-defined LIF measurements.[23] The purpose

of this work is to combine modelling and experimental approaches to extract useful informations to determine the axial electron mobility profile.

Results show that we are able to propose an analytical constant in time fit of the electron mobility that can reproduces the experimental features such that the electric field and ion distribution functions for a PPS®X000 for discharge voltages varying between 500 and 700 V. The paper is organized as the following, we come back to the previous method used to determine the axial electron mobility in section II. We briefly describe the PPS®X000 thruster in section III. The description of the hybrid model is presented in section III, while the main results are summarized in section IV. We finally end this paper with a conclusion in section V.

II. Direct measurement of the cross-magnetic field electron mobility

The electron mobility perpendicular to the magnetic field $\mu_{e,\perp}$ under the drift-diffusion approximation used in hybrid model is defined as :

$$\mu_{e,\perp}=\frac{j_{e,\perp}}{en_eE_\perp+e\nabla_\perp(n_eT_e)} \tag{1},$$

where e is the elementary electron charge, and n_e, T_e, and $j_{e,\perp}$, are the electron density, temperature, and cross-field current density, respectively. $\nabla_\perp$ symbolizes the cross-field gradient, and $E_\perp$ is the electric field perpendicular to the magnetic field.

The elementary theory links the cross magnetic field electron mobility to the total electron momentum transfer collision frequency ν_m and to the cyclotron angular frequency ω :

$$\mu_{e,\perp}=\frac{e}{m_e\nu_m}\frac{1}{1+(\omega/\nu_m)^2};\omega=\frac{eB}{m_e} \tag{2},$$

where m_e is the electron mass, and B is the magnetic field magnitude. Because $\omega >> \nu_m$, eq. (2) can be rearranged as:

$$\mu_{e,\perp}=\frac{1}{\Omega B} \tag{3},$$

where Ω is called the Hall parameter :

$$\Omega=\frac{\omega}{\nu_m} \tag{4}.$$

We can also rearrange eq. (1), the electron current being calculated from the current conservation current :

$$j_{e,\perp}=I_d/A-en_iV_{i,\perp} \tag{5}.$$

In eq. (5), I_d is the discharge current, A is the channel cross section area, n_i and $V_{i,\perp}$ are respectively the density and the mean velocity perpendicular to the magnetic field of ions.

Combining eqs. (1), (3) and (5), assuming a quasineutral plasma and neglecting the electron diffusion term, we can link the Hall parameter Ω (or electron cross field mobility) to I_d, B, $E_\perp$ n_e and $V_{i,\perp}$:

$$\frac{1}{\Omega}=B\frac{I_d/A-en_eV_{i,\perp}}{en_eE_\perp} \tag{6}.$$

Meezan *et al.*[5] have combined LIF diagnostic to determine the ion velocity profile and electrostatic probes to measure the electron density and the electric field profiles in order to obtain the Hall parameter variation. Note that the measurements have been achieved along the thruster centerline ; the perpendicular to the magnetic field direction in eq. (5) reduces to the axial direction in the region of strong magnetic field magnitude where the magnetic lens is convex.

We report in Figure 1 the measurements of Meezan *et al.*[5] for Hall thruster with a channel of 90 mm external diameter and 80 mm length. The xenon mass flow is 2.3 mg.s^{-1} and the discharge voltage V_d varies from 100 to 200 V. The "experimental" inverse Hall parameter profile has been derived from the plasma measured data, while the "classical" inverse Hall parameter profile assumes that only electron neural collisions participate to the momentum transfer [the Hall parameter being derived from eq. (4)]. In the estimation of the electron-neutral collision frequency $\nu_{e\text{-}n}$, the neutral density profile is deduced from LIF measurement of the neutral atom velocity (combined with the LIF ion velocity data) and the electron-neutral collision momentum rate is calculated assuming a Maxwellian distribution function for an electron temperature measured with probes.

The measurements presented in Figure 1 demonstrate without ambiguity the role of anomalous transport mechanism in the region of strong magnetic field and low neutral density. The authors correlate their measurements with the Bohm formulation of the anomalous transport[24] (τ being mean time between collisions). The large error bars observable in Figure 1 can be certainly a consequence of different factors : the number of data required, the use of intrusive probes perturbating the thruster operation, the difficulty to interpret the measurements in the region of strong magnetic field, etc. The accuracy of the measurements is insufficient to extract a quantitative axial profile of the Hall parameter and consequently of the cross field electron mobility that can be useful to simulate the thruster working.

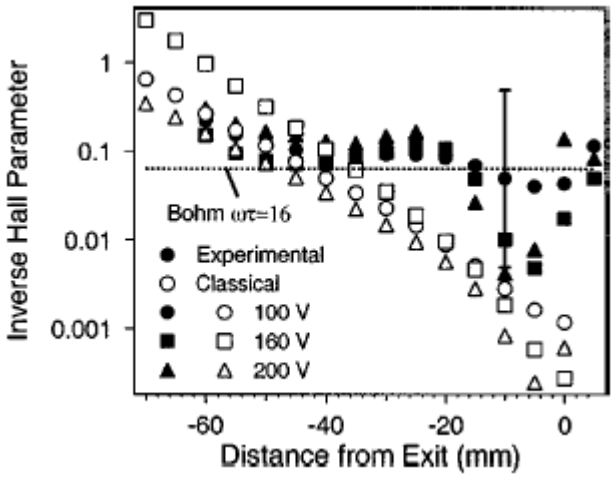

Figure 1 : Axial profile of the inverse Hall parameter.[5]

III. Brief overview of the PPS®X000 thruster

HETs used nowadays on board telecommunication satellites are in the range of 1-2 kW power. In the same range of power, the Smart-1 lunar mission of the European Space Agency has demonstrated that HETs can be employed for long duration mission.[2] During the operation, the PPS®1350 manufactured by Snecma has covered 100 millions of km during 16 months with 82 kg of xenon for a thrust of 70 mN. The necessary increase of the mass on board telecommunications satellites (e.g. Alphabus platform[25]), enabled by the increase of the payload carried by the launchers, requires high power HETs. Several 5 to 10 kW-class HETs have been manufactured and life-tested worldwide to be employed for North/South station keeping for such heavy-mass satellites (namely the NASA-173M in United States[26], the SPT-140 in Russia[27], and the PPS®X000 in Western Europe[28]). New types of mission like orbit transfer and manoeuvres of the satellites for high power HETs are expected too.

(a) (b)

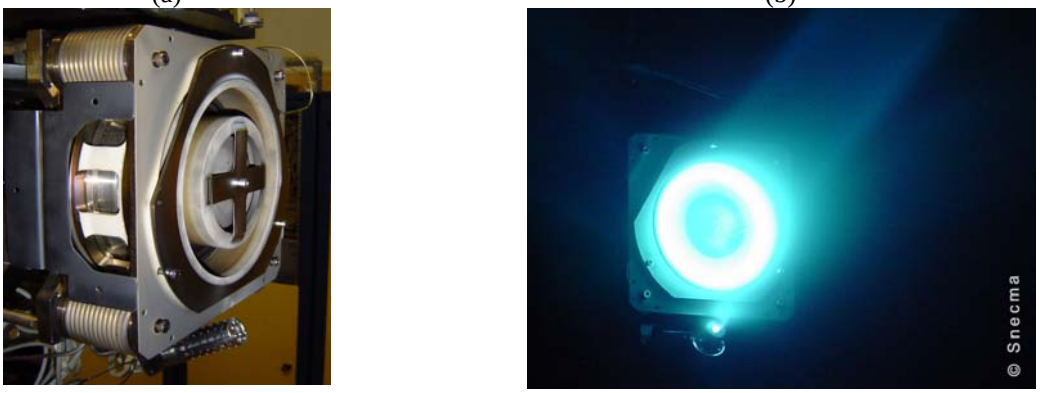

Figure 2 : (a) photo of the PPS®X000, (b) plume of the PPS®X000.

We present in Figure 2 a photo and a view of the plume of the PPS®X000. To test the PPS®X000, the pumping system in the PIVOINE facility (4 m long and 2.2 in diameter) in Orleans has been upgraded to reach a pumping speed of 150 000 l/s in xenon.[3] The PPS®X000 has been intensively tested in order to examine the possible dual-operation of the thruster (high specific impulse – low thrust for station keeping and low specific impulse – large thrust for orbit transfer).[29] During the study, the range of power was varying between 1 to 7 kW and the magnetic field was kept constant ; the mass flow rates varies from 5 to 15 mg.s^{-1} and the discharge voltage ranges from 200 to 1000 V. At 5 kW, the maximums of specific impulse or thrust were 2800 s or 260 mN, for a thruster efficiency around 0.5. The main conclusion of this study was that the PPS®X000 was able to operate at high thrust level, as desired.[28]

A laboratory version of the PPS®X000, namely the PPS®X000-LM, has been manufactured in order to characterize the discharge properties through LIF measurements.[21-22] A hole has been bored through the center of the anode plane so that a laser beam can pass in the direction parallel to the thruster channel. The external ceramic has a slit from 15 mm to the exit plane in order to collect the fluorescence signal inside the thruster channel. In the rest of the paper the exit plane is positioned at x = 0.

IV. Description of the hybrid model

The hybrid model is a transient two-dimensional code. The computational domain takes into account the channel and the near-outside region ; it extends on 10 cm in the axial direction x and 12 cm in the radial direction r. The cathode is positioned in the exit plane at r = 11 cm. The number of grid cells is 50 and 60 in the x and r directions, respectively. We begin this section by shortly describing in the sub-section A. the heavy species transport, in the sub-section B. we briefly come back to the treatment of the electron transport. The *ad hoc* hypothesis up to now used in the description of the cross magnetic field mobility of the electrons is detailed in sub-section C.

A. Ion and neutral transport

Xe singly-charged ions are generated by the ionization of the neutral atoms. The ionization rate is tabulated as a function of the electron mean energy assuming a Maxwellian electron distribution. We use the macro-particle technique as in Particle-In-Cell model, each macro-ion represents a certain number of individual ions (30 000 macro-ions are used) For simplicity reasons, we use the term ion for macro-ion in the rest of the section. The ion trajectories are integrated, the Newton Lorentz force reduces to the electric field component, ions being unaffected by the magnetic field due to their large mass and high velocity. Ions are followed until their leave the computational domain or impact on walls. Ions impinging walls are neutralized and a neutral atom is re-emitted isotropically assuming a half-Maxwellian distribution function with temperature of 500 K. A certain number of diagnostics such as the velocity distribution function has been also incorporated to compare the calculated distributions with the measured ones.

We use for xenon atoms the same technique as the ions using macro-atoms that account for a large number of individual atoms (typically 20 000 macro-atoms are simulated). The xenon neutral atoms are injected through a hole

in the anode plane assuming a Maxwellian distribution of the flux in the axial direction for a given temperature equal to 500 K. We also account for the background neutral atoms due to the backpressure tank by injecting an additional neutral flux at the thermal velocity (temperature of 300 K) from the boundaries of the computational domain in the near field region. Neutrals colliding with the walls are isotropically reflected back in the domain. Neutrals that exit the computational domain are not longer followed.

B. Electron transport

The electron fluid transport is described with the continuity, momentum and energy equations. The equation for the electron conservation is given by :

$$\frac{\partial n_e}{\partial t}+\nabla\cdot\mathbf{\Gamma}_e=S \tag{7},$$

where $\mathbf{\Gamma}_e$ is the electron flux, and S the ionisation source term.

The electron momentum equation is written – in the form of drift-diffusion approximation – as :

$$\mathbf{\Gamma}_e=\overline{\mu}\left(n_e\nabla V-\nabla\left(n_eT_e\right)\right) \tag{8}.$$

Due to the magnetic field, the mobility $\overline{\mu}$ is not a scalar but a tensor[30], where the component parallel to the magnetic field is given by the following relation :

$$\mu_{e,//}=\frac{e}{m_e\nu_m} \tag{9}.$$

The component perpendicular to the magnetic field is given by the eq. (2).

Combining eqs. (7) and (8), and assuming quasineutrality ($n\approx n_i\approx n_e$) since were are not interested in the description of cathode and anode sheaths, the electric potential V is calculated solving the following elliptic equation:

$$\nabla.\mathbf{\Gamma}_e=\nabla.\left[\overline{\mu}\left(n\nabla V-\nabla\left(nT_e\right)\right)\right]=\nabla.\mathbf{\Gamma}_i \tag{10}.$$

In eq. (10), the plasma density n as well as the ion flux $\mathbf{\Gamma}_i$ are deduced from the ion transport. The numerical method used to solve eq. (10) is presented by Hagelaar.[31]

The Boundary conditions are fixed potential at the cathode V_c=0 and at the anode V_a=V_d – where V_d is the discharge voltage. The electric potential is fixed to 0 on the open frontier of the computational domain. We impose on the dielectric walls, on the front plane an equality between the electron flux $\mathbf{\Gamma}_e$ and the ion flux $\mathbf{\Gamma}_i$.

In order to determine the electron temperature T_e (or the electron mean energy $\varepsilon=3/2\beta T_e$ - β is the Boltzmann factor) to calculate the ionization rate, we solve an energy equation :

$$\frac{\partial(n\varepsilon)}{\partial t}+\frac{5}{3}\nabla\cdot(\mathbf{\Gamma}_e\varepsilon)-\frac{10}{9e}\nabla\cdot(\mu n\varepsilon\nabla\varepsilon)=e\mathbf{\Gamma}_e.\nabla V-Nn\kappa-nW \tag{11},$$

N being the neutral gas density. The last two terms in the energy equation represent energy loss by collisions with gas particles and with the walls, respectively, where κ and W are effective energy loss coefficients[32].

C. *Ad hoc* formulation of the cross field electron mobility

Up to now, in the hybrid model, the total electron momentum transfer frequency ν_m is an effective collision frequency including the electron-atom collisions (frequency $\nu_{e\text{-}n}$), electron-ion collisions (frequency $\nu_{e\text{-}i}$), electron-wall collisions (frequency $\nu_{e\text{-}w}$), and Bohm-like transport (frequency ν_{Bohm}). The total electron momentum transfer frequency in eq. (2) is written as the sum of each contribution, therefore, $\nu_m = \nu_{e\text{-}n} + \nu_{e\text{-}i} + \nu_{e\text{-}w} + \nu_{Bohm.}$[4-6, 14-15] The momentum transfer frequency collision between electrons and atoms $\nu_{e\text{-}n}$ is inferred from the neutral density profile and the electron-atom momentum transfer rate that is assumed constant (k_m = 2.5×10^{-13} m^3s^{-1}). The effect of

electron-ion collisions on the momentum transfer is deduced from the Coulomb cross sections assuming a Maxwellian electron distribution function.[33] We account for wall effects inside the thruster channel with a collision frequency equal to $\nu_{e\text{-}w} = \alpha \nu_{ref}$ (with $\nu_{ref} = 10^7 s^{-1}$). Notice that some authors use refine theories to account for secondary electron emission under high energetic electron impacts on the ceramic walls.[7,9-10] We assume that the anomalous transport is governed outside the channel by Bohm-like transport with an equivalent collision frequency $\nu_{Bohm} = K\Omega/16$. The two parameters α and K are adjusted in order to match experimental integrated measurements (performance, ionization efficiency, current and its time variation, etc.).[15] We can remark that electron-wall collisions does not depend of the magnetic field, consequently, the mobility varies as $1/B^2$ like the "classical" collision mobility, while Bohm-like transport, leads to a mobility varying as $1/B$.

Scharfe *et al.*[9] have compared the plasma modeling results when the Bohm or the experimental (discussed in section II - see Fig. 5) mobility is assumed, the authors conclude that the experimental mobility leads to plasma properties in better agreement with experimental results obtained for the Stanford Hall thruster. Koo and Boyd[8] have also compared the *ad hoc* Bohm-type assumed anomalous transport with a deduced mobility profile from measurements (combined with some modeling assumptions due to the lack of the electron current density measurements). Koo and Boyd find a better agreement of the overall behavior of the UM/AFRL P5 Hall thruster of 5 kW is observed when the experimental mobility profile is used. Following the same idea, the goal of the paper is to compare the *ad hoc* hypothesis of the anomalous transport with the reconstructed mobility profile obtained from LIF measurements for the PPS®X000-LM.

V. Results and discussion

In sub-section A, we test the model *ad hoc* hypothesis on the electron mobility comparing the experimental and calculated ion velocity profiles for the PPS®X000-LM. In sub-section B, we examine the influence of the discharge voltage on the ion velocity distribution functions. In all this study the coil currents (17 A) and the xenon mass flow (6 $mg.s^{-1}$) remain the same.

A. Mobility profile

In Figure 3a, the experimental as well as the simulated time-averaged on-axis profiles of the axial electric field are shown together with the computed ionization source term for a discharge voltage of 500 V. In the calculations indicated as hybrid # 1, we represent the anomalous electron transport mechanisms taking into account wall effects inside the channel with a collision frequency equal to $\nu_{e\text{-}w} = \alpha \nu_{ref}$ (with $\nu_{ref} = 10^7 s^{-1}$), and outside the channel Bohm-like transport with an equivalent collision frequency $\nu_{Bohm} = K\Omega/16$. The adjustable coefficients are $\alpha = 1.45$ and $K = 0.2$, as in the work of Boniface *et al.*[14] The electron mobility profile calculated with eq. (1) is plotted in Fig. 3b. Clearly there is no agreement with experiments (see Fig. 3b). The use of empirical laws with $1/B^2$ (or $1/B$ – not shown here) mobility inside the channel and $1/B$ outside the channel as we have previously done with tunable coefficients do not allow us to reproduce the measured profile of axial ion velocity.

The reason is clearly associated to the misestimating of the electric field profile. The method employed to extract electric field profile from measurements is detailed in the paper of Pérez-Luna *et al.*[23] In the measurements, the maximum of electric field reaches 35 $kV.m^{-1}$, while the calculations give a maximum of electric field in order of only 20 $kV.m^{-1}$. We also see that the length of the acceleration layer is typically few millimeters in the experiments, while it extends on more than one centimeter in the calculations. Consequently, the experimental ion velocity profile differs from the calculated one.

In the calculations labeled as hybrid # 2, we have adjusted the anomalous electron mobility profile in order to match the experimental profile of the axial ion velocity (see Fig. 3b). The shape of calculated axial electric profile presented in Fig. 3a is now in agreement with the profile deduced from LIF measurements. Integrating the measured axial electric field profile leads to a potential drop much smaller than the discharge voltage (sheath falls). This explains the shift between the simulated and measured most probable velocity (see Fig. 4). The fitted electron mobility profile (depending on the axial position) shown in Fig. 3b is in qualitative agreement with the measured profile in the P5 thruster[8]. Empirical laws with $1/B^2$ or $1/B$ mobility (see Fig. 3b - hybrid # 1) differ by far from the analytical profile.

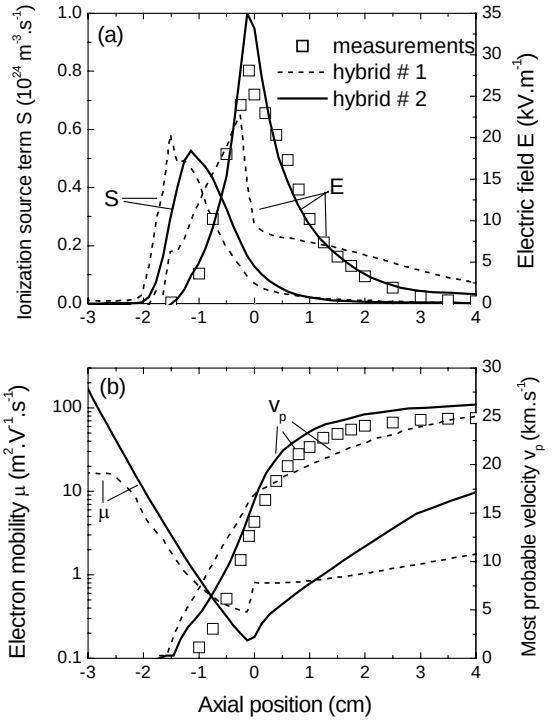

Figure 3 : Time-averaged profiles along the PPS®X000-LM thruster channel axis of (a) the electric field deduced from LIF measurements and the computed electric field profile and the calculated ionization source term, (b) the electron mobility perpendicular to the magnetic field and most probable ion velocity. Conditions are : V_d = 500 V, m_a = 6 mg.s^{-1}. The coil currents is fixed to 17 A. The channel exit is at x = 0.

B. Ion velocity distribution functions

We present in the Figure 4 the experimental and calculated IVDFs at the end of the acceleration layer at x = 4 cm (the reference axial position x = 0 is at the exit plane). Part of the broadening of the IVDFs is associated to the overlap between the ionization and acceleration layers that is visible in the Figure 3a. We have already noticed that transient evolution of the plasma also influences the shape of the IVDFs. The choice of tuned coefficients in the elementary laws (*1/B*^{2} or *1/B*) used so far in hybrid models has strongly influenced the dynamic behavior of the discharge, especially the magnitude of transit-time oscillations. The transit-time oscillations (100-500 kHz) are associated to the time needed by the ions to cross the acceleration layer. The visible consequence was noticed in the shape of IVDFs at the end of the acceleration layer where a large velocity dispersion was obtained[4, 15].

In Figure 4a, we show the calculated and the measured IVDFs of the PPS®X000-LM thruster for discharge voltages in the range of 500-700 V. The empirical mobility profile is the same as in Fig. 3b. The calculated IVDFs now match the measured IVDFs (especially the broadening of the distribution). This suggests that the high-frequency dynamic behavior is correctly represented in the model. The theoretical maximum axial velocity an ion can reach for a given discharge voltage V_d is $v_{max} = (2eV_d/m_{Xe+})^{1/2}$ where m_{Xe+} is the ion mass. Both model and experiments confirm the existence of very fast ions with a velocity larger than v_{max} in the final part of the acceleration layer. This is clearly attributed to a "wave riding" phenomenon that makes possible for the ions to acquire a kinetic energy larger than the given potential energy $e \times V_d$.[4,15, 20, 22] Conserving a given profile of the cross field electron mobility leads also to reasonable describe the thruster working.

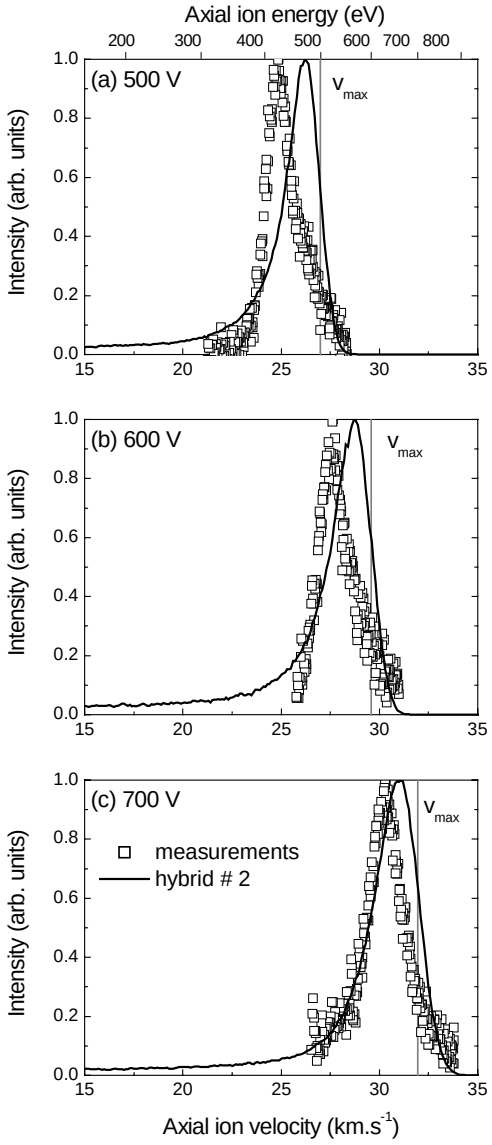

Figure 4 : IVDFs obtained by LIF measurements[22] and calculated with the PPS®X000-LM at x = 4 cm for (a) V_d = 500 V, (b) V_d = 600 V, and (c) V_d = 700 V, and for m_a = 6 mg.s^{-1}. The coil currents is 17 A. The theoretical maximum axial velocity v_{max} is also shown.

VI. Conclusions and future work

In this paper, we have demonstrated that one single diagnostic such that laser spectroscopy technique is able to provide indirect informations on the axial electron mobility profile. Results show that previous elementary laws (*1/B*^{2} or *1/B*) with adjusted coefficients in order to match the correct "macroscopic" properties of the thruster (current, power, performance) used so far in hybrid models fail to reproduce experimental observations such that as the measured ion velocity profile. Fitting the calculated ion velocity profiles with the LIF measurements obtained at 500 V leads to a empirical steady spatial profile of the axial electron mobility that is able to reproduce the thruster properties and the measured ion velocity distribution functions, in the wide range of discharge voltages for the PPS®X000-LM thruster. The hybrid model is still unfortunately non-self consistent.

The adjusted electron mobility profile in this study is in qualitative agreement with the calculated electron mobility from PIC simulations[12]. We now plan to use the PIC model in order to identify and understand the physical

parameters that govern the anomalous electron transport. We also want to deduce from these calculations scaling laws of the electron mobility as a function of the discharge parameters in order to propose a less empirical description of the electron mobility in the hybrid model.

Acknowledgments

This work is performed in the frame of the joint-research program CNRS/CNES/Sncema/Universités n° 3161 "Propulsion par Plasma dans l'Espace" and by the TELIOPEH ("*Transport ELectronique et IOnique dans les Propulseurs à Effet Hall*") project, funded by ANR (National Research Agency), under contract ANR-06-BLAN-0171. J. Pérez-Luna has benefited from a CNES/Snecma PhD fellowship.

References

[1] V.V. Zhurin, H.R. Kaufman, and R.S. Robinson, "Physics of Closed Drift Thrusters", *Plasma Sources Sci. Technol.* Vol. 8**,** No. 1, 1999, R1-R20.

[2] C. Koppel, F. Marchandise, D. Estublier, and L. Jolivet, "The Smart-1 Electric Propulsion Subsystem in Flight Experience", *Proceedings of the 40th AIAA Joint Propulsion Conference and Exhibit*, Fort Lauderdale, FL, 11-14 July 2004, paper AIAA-2004-3435.

[3] S. Mazouffre, A. Lazurenko, P. Lasgorceix, M. Dudeck, S. d'Escrivan, and O. Duchemin, "Expanding Frontiers : Towards High Power Hall Effect Thrusters for Interplanetary Journeys", *Proceedings of the 7th International Symposium on Launcher Technologies*, April 2-5 2007, Barcelona, Spain, Paper O-25 (2007).

[4] G.J.M. Hagelaar, J. Bareilles, L. Garrigues, and J.P. Boeuf, "Role of Anomalous Electron Transport in a Stationary Plasma Thruster Simulation", *J. Appl. Phys*., Vol. 93, No. 1, 2003, 67-75.

[5] N. Meezan, W. Hargus, and M. Capelli, "Anomalous Coaxial Electron Mobility in a Coaxial Hall Discharge Plasma", *Phys. Rev. E*, Vol. 63, No. 2, 2001, 026410 (7 pp).

[6] G.S. Janes and R.S. Lowder, "Anomalous Electron Diffusion and Ion Acceleration in a Low-Density Plasma", *Phys. Fluids*, Vol. 9, No. 6, 1966, 1115-1123.

[7] S. Barral, K. Makowski, Z. Peradzyński, N. Gascon, and M. Dudeck, "Wall Material Effects in Stationary Plasma Thrusters. II. Near-Wall and In-Wall Conductivity", *Phys. Plasmas*, Vol.10, No. 10, 2003, 4137-4152.

[8] J.W. Koo and I.D. Boyd, "Modeling of Anomalous Electron Mobility in Hall Thrusters", *Phys. Plasmas*, Vol. 13, No. 3, 2006, 033501 (7 pp).

[9] M.K. Scharfe, N. Gascon, M.A. Cappelli, and E. Fernandez, "Comparison of Hybrid Hall Thruster Model to Experimental Measurements" *Phys. Plasmas*, Vol. 13, No. 8, 2006, 083505 (12 pp).

[10] F.I. Parra, E. Ahedo, J.M. Fife, and M. Martinez-Sanchez, "A Two-Dimensional Hybrid Model of the Hall Thruster Discharge", *J. Appl. Phys.*, Vol. 100, No. 2, 023304 (11 pp).

[11] J.C. Adam, A. Heron, and G. Laval, "Study of Stationary Plasma Thrusters using Two-Dimensional Fully Kinetic Simulations", *Phys. Plasmas*, Vol. 11, No. 1, 2004, 295-305.

[12] J.C. Adam, J.P. Boeuf, N. Dubuit, M. Dudeck, L. Garrigues, D. Gresillon, A. Heron, G.J.M. Hagelaar, V. Kulaev, N. Lemoine, S. Mazouffre, J. Pérez-Luna, V. Pisarev, and S. Tsikita, "Physics, Simulation and Diagnostics in Hall Thrusters", *Plasma Phys. Control. Fusion*, Vol. 50, No. 12, 2008, 1214041 (17 pp).

[13] S. Tsikita, N. Lemoine, V. Pisarev, and D.M. Gresillon, "Dispersion Relations of Electron Density Fluctuations in a Hall Thruster plasma, Observed by Collective Light Scattering, *Phys. Plasmas*, Vol. 16, No. 3, 2009, 033506 (10 pp).

[14] C. Boniface, L. Garrigues, G.J.M. Hagelaar, J.P. Boeuf, D. Gawron, and S. Mazouffre, "Anomalous Cross Field Electron Transport in a Hall Effect Thruster", *Appl. Phys. Lett.* , Vol. 89, No. 16, 2006, 161503 (3 pp).

[15] J. Bareilles, G.J.M. Hagelaar, L. Garrigues, C. Boniface, J.P. Boeuf, and N. Gascon, "Critical Assessment of a Two-Dimensional Hybrid Hall Thruster Model : Comparisons with Experiments", *Phys. Plasmas*, Vol. 11, No. 6, 2004, 3035-3046.

[16] W.A. Hargus, Jr. and M.A. Capelli, "Laser-Induced Fluorescence Measurements of Velocity Within a Hall Discharge",. *Appl. Phys. B*, Vol. 72, No. 8, 2001, 961-969.

[17] N. Dorval, J. Bonnet, J.P. Marque, E. Rosencher, S. Chable, F. Rogier, and P. Lasgorceix, "Determination of the Ionization and Acceleration Zones in a Stationary Plasma Thruster by Optical Spectroscopy Study : Experiments and Model", *J. Appl. Phys.*, Vol. 91, No. 9, 2002, 4811-4817.

[18] W.A. Hargus, Jr. and C. S. Charles, "Near Exit Plane Velocity Field of a 200-Watt Hall Thruster", *J. Propul. Power*, Vol. 24, No. 1, 2008, 127-133.

[19] W.A. Hargus, Jr. and M.R. Nakles, "Ion Velocity Measurements Within the Acceleration Channel of a Low-Power Hall Thruster", *IEEE Trans. Plasma Sci*., Vol. 36, No. 5, 2008, 1989-1997.

[20] D. Gawron, S. Mazouffre, N. Sadeghi, and A. Héron, "Influence of Magnetic Field and Discharge Voltage on the Acceleration Layer Features in a Hall Effect Thruster", *Plasma Sources Sci. Technol.*, Vol. 17, No. 2, 2008, 025001 (10 pp).

[21] S. Mazouffre, D. Gawron, V. Kulaev, and N. Sadeghi, "Xe^+ Ion Transport in the Crossed-Field Discharge of a 5-kW-Class Hall Effect Thruster", *IEEE Trans. Plasma Sci.*, Vol. 36, No. 5, 2008, 1967-1976.

[22] S. Mazouffre, V. Kulaev, and J. Pérez-Luna, "Ion Diagnostics of a Discharge in Crossed Electric and Magnetic Fields For Electric Propulsion", *Plasma Sources Sci. Technol.*, Vol. 18, No. 3, 2009, 034022 (12 pp).

[23] J. Pérez-Luna, G.J.M. Hagelaar, L. Garrigues, and J.P. Boeuf, "Method to Obtain the Electric Field and the Ionization Frequency from Laser Induced Fluorescence Measurements", *Plasma Sources Sci. Technol.*, Vol. 18, No. 3, 2009, 034008 (6 pp),
[24] D. Bohm, in *The Characteristics of Electrical Discharges in Magnetic Fields*, edited by A. Guthrie and R. K. Wakerling, McGraw-Hill, New York, 1949, Chap. 2, p. 65.
[25] M. Roux and P. Bertheux, "Alphabus, the European Platform for Large Communication Satellites", *Proceedings of the 25th AIAA International Communications Satellite Systems Conference*, Seoul, South-Korea, 10-13 April 2007, paper AIAA-2007-3121.
[26] R.R. Hofer, R.S. Jankovsky, and A.D. Gallimore, "High-Specific Impulse Hall Thrusters, Part 1 : Influence of Current Density and Magnetic Field", *J. Propul. Power*, Vol. 22, No. 4, 2006, 721-731.
[27] A. Lazurenko, V. Vial, A. Bouchoule, A. Skrylnikov, V. Kozlov, and V. Kim, "Dual-Mode Operation of Stationary Plasma Thrusters", *J. Propul. Power*, Vol. 22, No. 1, 2006, 38-47.
[28] O. Duchemin, N. Cornu, F. Darnon, and D. Estublier, "The Smart-1 Electric Propulsion Subsystem in Flight Experience", *Proceedings of the 41st AIAA Joint Propulsion Conference and Exhibit*, Tucson, AZ, 10-13 July 2005, paper AIAA-2005-4050.
[29] O. Duchemin, P. Dumazert, D. Estublier, F. Darnon, and N. Cornu, "Stretching the Operational Envelope of the PPS®X000 Plasma Thruster", *Proceedings of the 40th AIAA Joint Propulsion Conference and Exhibit*, Fort Lauderdale, FL, 11-14 July 2004, paper AIAA-2004-3605.
[30] M.A. Lieberman and A.J. Lichtenberg, *Principles of Plasma Discharges and Materials Processing*, 2nd ed., Wiley, Hoboken, 1994, Chap. 5.
[31] G.J.M. Hagelaar, "Modelling Electron Transport in Magnetized Low Temperature Discharge Plasmas", *Plasma Sources Sci. Technol.*, Vol. 16, No. 1, 2007, pp. S57-S66.
[32] G.J.M. Hagelaar, J. Bareilles, L. Garrigues, and J.P. Boeuf, "Two Dimensional Model of a Stationary Plasma Thruster", *J. Appl. Phys.*, Vol. 91, No. 9, 2002, pp. 5592-5598.
[33] B.E. Cherrington, *Gaseous Electronics and Gas Lasers*, Pergamon Press, New York, 1979.